



Identifying nonlinear dynamics of brain functional networks of patients with schizophrenia by sample entropy

Yanbing Jia · Huaguang Gu

Received: 23 November 2018 / Accepted: 27 March 2019 / Published online: 1 April 2019
© Springer Nature B.V. 2019

Abstract Different regions in the human brain functionally connect with each other forming a brain functional network, and the time evolution of functional connectivity between different brain regions exhibits complex nonlinear dynamics. This study intends to characterize the nonlinear properties of dynamic functional connectivity and to explore how schizophrenia influences such nonlinear properties. The dynamic functional connectivity is constructed by analyzing resting-state functional magnetic resonance imaging data, and its nonlinear properties are characterized by sample entropy (SampEn), with larger SampEn values corresponding to more complexity. To identify the influence of schizophrenia on SampEn, the difference in SampEn between patients with schizophrenia and healthy controls is analyzed at different levels of the brain. It is shown that the patients exhibit significantly higher SampEn at different levels of the brain, and such phenomenon is mainly caused by a significantly higher SampEn in the visual cortex of the patients. Further-

more, it is also shown that SampEn of the visual cortex is significantly and positively correlated with the illness duration or the symptom severity scores. Because the visual cortex is implicated in the visual information processing, these results can shed light on abnormal visual functions of patients with schizophrenia, and also are consistent with the notion that the nonlinearity underlies the irregularity in psychotic symptoms of schizophrenia. This study extends the application of nonlinear dynamics in brain sciences and suggests that nonlinear properties are effective biomarkers in characterizing the brain functional networks of patients with brain diseases.

Keywords Sample entropy · Nonlinear dynamics · Dynamic functional connectivity · Brain functional networks · Schizophrenia

1 Introduction

The human brain, a complex nonlinear system with hierarchical levels, exhibits complex spatiotemporal behaviors at different hierarchical levels when executing physiological functions or suffering from diseases. Identifying nonlinear dynamics of the spatiotemporal behaviors which dynamically evolve over time is an important approach to understand the human brain. In single neurons, many nonlinear behaviors, such as typical chaos and bifurcations of neuronal firing patterns, have been observed in biological experiments

This work was sponsored by the National Natural Science Foundation of China (Grant Numbers: 11802086, 11872276, and 11572225) and the Key Project of Higher Learning Institution of Henan (Grant Number: 19A110014).

Y. Jia
School of Mathematics and Statistics, Henan University of Science and Technology, Luoyang 471023, China

Y. Jia · H. Gu (✉)
School of Aerospace Engineering and Applied Mechanics, Tongji University, Shanghai 200092, China
e-mail: guhuaguang@tongji.edu.cn

and analyzed in theoretical models [1–5]. In neuronal networks, multiple spatiotemporal behaviors, such as synchronizations and spiral waves, have been observed in biological experiments and simulated in theoretical models [6–10]. For the human brain, blood oxygen level-dependent (BOLD), electroencephalography (EEG), magnetoencephalography (MEG), and electrocorticogram (ECoG) signals of different brain areas can be measured in biological or clinical experiments and can be analyzed by the method of time series analysis to characterize spatiotemporal dynamics of the human brain. Because of the difficulty in modeling the human brain and the lack of understanding about the nonlinear dynamics of the human brain, theoretical models describing nonlinear dynamics of the human brain have been put little attention. In spite of this, the method of nonlinear time series analysis has been used to analyze the spatiotemporal behaviors of BOLD, EEG, MEG, and ECoG signals [11–19], which may be useful for modeling a brain showing nonlinear dynamics [20].

Since BOLD signals of the human brain can be measured at a spatial resolution of about 3 mm^3 (a voxel) by functional magnetic resonance imaging (fMRI) technique, analyzing the dynamics of BOLD signals at different hierarchical levels, such as the voxel level and the regional level, has been broadly used to understand brain functions and brain diseases [21–23]. For example, researchers have shown that some measures obtained by analyzing the dynamics of BOLD signals, such as the temporal correlation in BOLD signals of different voxels or brain regions, can be used as objective indicators for characterizing brain conditions such as schizophrenia [24], autism [25], major depressive disorder [26], and attention deficit hyperactivity disorder [27]. Analyzing the dynamics of BOLD signals of healthy individuals and patients with brain diseases measured by resting-state and task-based fMRI as well as introducing new methods to analyze the dynamics of BOLD signals is important issue in the study of BOLD signals.

In the study of BOLD signals, three typical hierarchical levels of the human brain are the voxel level, the regional level, and the network level. These three hierarchical levels are interrelated. Specifically, a brain region is composed of many voxels, whereas a network is composed of many brain regions. The dynamics of BOLD signals at these three hierarchical levels can be used to describe the dynamical evolution of the human brain. For example, the temporal correlation in

resting-state fMRI BOLD signals of different voxels or brain regions has been widely used to characterize the functional connectivity between them [28], and voxels or brain regions with strong functional connectivity among them have been considered to constitute a brain functional network [29]. If a brain functional network is changed in subjects with specific brain condition, brain regions in this brain functional network are considered to be related to this brain condition. For example, by analyzing functional connectivity between different voxels or between different brain regions in subjects with autism, Cheng et al. found an important system in the middle temporal gyrus with decreased functional connectivity, which is involved in social behavior, as well as an important system in the precuneus with decreased functional connectivity, which is involved in spatial functions [30]. Schizophrenia is another specific brain condition, which is characterized by positive symptoms such as hallucinations and delusions, and negative symptoms such as social withdrawal and apathy [31]. Functional connectivity analysis on resting-state BOLD signals suggested that the abnormal properties of functional connectivity were important features of schizophrenia [32–36]. For instance, Manoliu et al. showed that the functional connectivity between the default mode network and the central executive network was increased in patients with schizophrenia, which was also related with hallucinations severity [35]. Whitfield-Gabrieli et al. showed that patients with schizophrenia displayed abnormally high functional connectivity within the default mode network, which resulted in the disorganized thinking in schizophrenia [36].

In most previous studies on functional connectivity, only one correlation coefficient was obtained for the BOLD signals of two brain regions, which is termed as static functional connectivity. Recently, to identify the dynamics of BOLD signals more in depth, researchers obtained a series of correlation coefficients by the sliding-window correlation technique, which was performed by evaluating correlation coefficient between the BOLD signals of two brain regions within a short time window, then sliding the window from the beginning to the end of the BOLD signals [37]. The time series of correlation coefficients, which is called as dynamic functional connectivity, can characterize the time-varying properties of functional connectivity [37–44]. For example, by evaluating dynamic functional connectivity between different brain regions,

Allen et al. showed that some functional connections, such as the functional connections between the lateral parietal cortex and the cingulate cortex, were more dynamic or flexible [37]. Furthermore, except for linear properties characterized by static or dynamic functional connectivity, nonlinear properties of BOLD signals were identified in previous studies [12, 14–16, 18], which is in line with the fact that the brain is a complex nonlinear system. For instance, Wang et al. used sample entropy (SampEn) to characterize nonlinear properties of resting-state BOLD signals collected from a large cohort of healthy individuals, and found that different brain regions show different SampEn values [14]. Sokunbi et al. calculated SampEn of BOLD signals collected from patients with schizophrenia and healthy controls while performing the cyberball social exclusion task, and found that patients exhibited significantly higher SampEn than that of the controls [16]. Therefore, dynamic functional connectivity analysis and nonlinear analysis are highly effective methods for characterizing properties of the human brain. In our recent study [45], nonlinear analysis of dynamic functional connectivity is used to study properties of the brain functional networks. Specifically, the relationship between SampEn of dynamic functional connectivity and age was investigated. It was shown that SampEn of the amygdala–cortical functional connectivity was negatively correlated with age, and such relationship disappeared in patients with schizophrenia.

Considering that the influence of schizophrenia on SampEn of dynamic functional connectivity at different levels of the brain was not investigated in Ref. [45], the present study intends to investigate whether SampEn of dynamic functional connectivity is changed in patients with schizophrenia and whether this change is related to symptoms of schizophrenia. It is shown that the patients with schizophrenia exhibit significantly higher SampEn than the healthy controls at different levels of the brain, and such phenomenon is mainly caused by a significantly higher SampEn in the visual cortex of the patients with schizophrenia. Furthermore, it is also shown that SampEn of the visual cortex is significantly and positively correlated with the illness duration or the symptom severity scores. The results are helpful for understanding the characteristics of schizophrenia, extending the applications of nonlinear dynamics, and strengthening the combination of nonlinear dynamics and neuroscience.

The present study is structured as follows: The experiments and methods are displayed in Sect. 2. The difference in SampEn between the patients with schizophrenia and the healthy controls, as well as the relationship between SampEn and symptoms of schizophrenia, is shown in Sect. 3. The conclusion and discussion are described in Sect. 4.

2 Experiments and methods

2.1 Participants

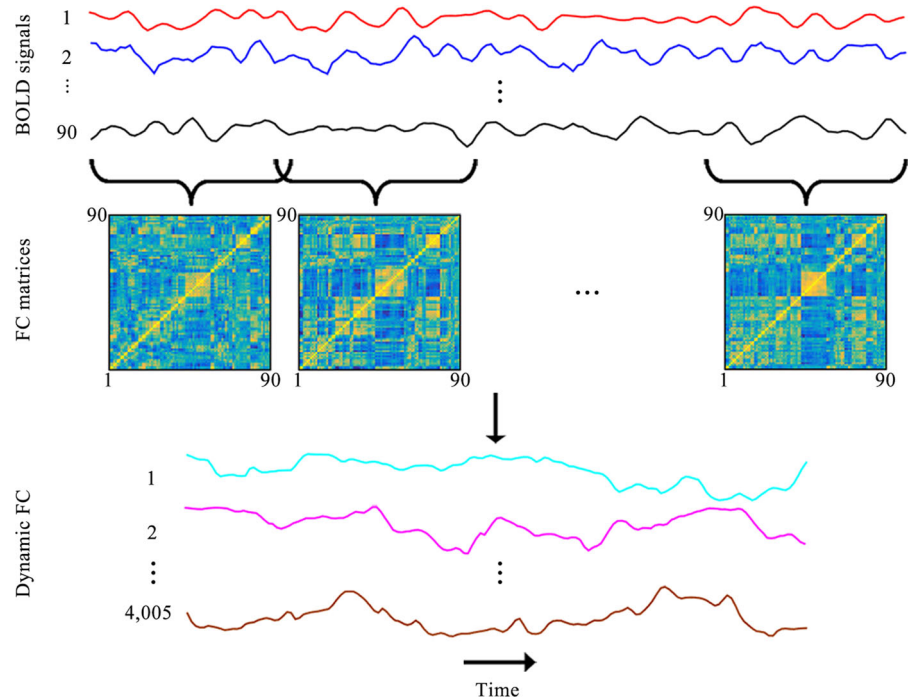
BOLD signals included in the present study are taken from a previous study about abnormal static functional connectivity in patients with schizophrenia [33] and are the same as that used in Ref. [45]. BOLD signals are collected from 69 patients with schizophrenia and 62 healthy controls. Written informed consent is acquired from each participant. All patients are identified by qualified psychiatrists according to criteria in 4th edition of Diagnostic and Statistical Manual of Mental Disorders (DSM-IV). All controls are assessed by qualified psychiatrists as being free of schizophrenia and other brain disorders in accordance with criteria in DSM-IV. The symptom severity of each patient is evaluated by positive and negative syndrome scales (PANSS). However, 5 patients cannot finish their evaluation due to their poor health. Experimental procedures are approved by National Taiwan University Hospital institutional review boards.

2.2 Data acquisition and preprocessing

BOLD signals are extracted from whole-brain functional images, which are acquired on a Siemens 3 Tesla MRI scanner. The parameters are as follows: repetition time, 2000 ms; echo time, 24 ms; field of view, $256 \times 256 \text{ mm}^2$; matrix, 64×64 ; axial slices, 34; slice thickness, 3 mm; flip angle, 90° . During the image collection, all participants are asked to rest while awake. For each participant, a total of 180 whole-brain functional images are acquired.

Preprocessing of functional images is conducted by SPM software [46] and DPARSF software [47]. Details of the preprocessing are as follows: Firstly, the first 10 images are deleted to decrease the negative influence of scanner's stabilization on experimen-

Fig. 1 Dynamic functional connectivity estimated using the sliding-window approach. For each participant, the BOLD signal of each region of interest is first calculated. Dynamic functional connectivity matrices are then estimated using the sliding-window approach. Finally, dynamic functional connectivity between each pair of regions of interest is obtained from the functional connectivity matrices. FC: functional connectivity



tal results. Secondly, the images are corrected for time delays between different slices as well as rigid-body head motion. Thirdly, the images are normalized to the Montreal Neurological Institute template and are resampled to $3 \times 3 \times 3 \text{ mm}^3$. Fourthly, the images are smoothed by a Gaussian kernel (full width at half maximum = 8 mm). Fifthly, the BOLD signal of each voxel is extracted from the images and then is band-pass-filtered (0.01 – 0.08 Hz) to decrease the negative influence of low-frequency drift and high-frequency physiological noise on experimental results. Finally, covariates are regressed out from the BOLD signal of each voxel, including six head-motion parameters, the global, the white matter, and the cerebrospinal signals.

2.3 Method of estimating dynamic functional connectivity: the sliding-window correlation analysis

The whole brain is parceled out into 90 regions of interest using the automated anatomical labeling atlas [48]. The full name of each region of interest can be found in Table S1 of Ref. [45]. For each region of interest, the BOLD signal is calculated by averaging BOLD signals of all voxels in the region of interest (Fig. 1). The number of voxels in each of 90 regions of interest is

provided in Table 1, and the number ranges from 62 to 1510. Dynamic functional connectivity is estimated using the sliding-window approach [37]. Specifically, a rectangle window with a length of 40 s is constructed. This window is applied to extract time series in steps of 2 s, resulting in 150 time windows per participant. For each time window, a Pearson correlation coefficient is used to assess functional connectivity between each pair of regions of interest. Functional connectivity matrices are thus obtained for each participant (Fig. 1). Dynamic functional connectivity between each pair of regions of interest is then obtained from the functional connectivity matrices (Fig. 1). Throughout this study, the window length is fixed at 40 s. This window length is selected because previous studies showed that window lengths ranging from 30 s to 60 s produced robust results in data acquisitions [49], and changes of functional connectivity were not sensitive to window lengths ranging from 20 s to 40 s [50].

2.4 Method of calculating SampEn of a dynamic functional connectivity time series

If a dynamic functional connectivity time series is denoted by $\mathbf{x} = (x_1, x_2, \dots, x_N)$ ($N = 150$), SampEn of \mathbf{x} can be calculated as follows [45].

Table 1 The mean SampEn of each region of interest over all controls and over all patients. The data are shown in ascending order according to p values of t tests on SampEn of the two groups. The number of voxels in each region of interest is also provided. The full name of each region of interest can be found in Table S1 of Ref. [45]

Regions of interest	SampEn of patients	SampEn of controls	p value	Number of voxels
ROL.R	0.5354 ± 0.0458	0.5048 ± 0.0359	0.0009*	399
MOG.L	0.5263 ± 0.0380	0.5037 ± 0.0433	0.0014*	959
MOG.R	0.5351 ± 0.0387	0.5094 ± 0.0399	0.0024*	595
IOG.R	0.5352 ± 0.0420	0.5110 ± 0.0379	0.0033*	314
SOG.L	0.5242 ± 0.0424	0.5060 ± 0.0349	0.0057*	396
PAL.R	0.5381 ± 0.0381	0.5183 ± 0.0404	0.0062	76
PCG.R	0.5361 ± 0.0384	0.5167 ± 0.0443	0.0072	87
SFGdor.L	0.5307 ± 0.0399	0.5096 ± 0.0398	0.0076	1076
SPG.R	0.5286 ± 0.0442	0.5065 ± 0.0389	0.0081	647
PAL.L	0.5390 ± 0.0436	0.5206 ± 0.0424	0.0131	81
IOG.L	0.5229 ± 0.0367	0.5057 ± 0.0395	0.0204	268
SOG.R	0.5292 ± 0.0448	0.5065 ± 0.0360	0.0206	428
INS.L	0.5308 ± 0.0465	0.5154 ± 0.0379	0.0232	566
ACG.R	0.5250 ± 0.0464	0.5049 ± 0.0391	0.0239	397
PoCG.R	0.5237 ± 0.0457	0.5037 ± 0.0418	0.0270	1138
STG.L	0.5283 ± 0.0417	0.5099 ± 0.0368	0.0270	672
IFGtriang.L	0.5241 ± 0.0366	0.5116 ± 0.0417	0.0461	726
OLF.R	0.5427 ± 0.0466	0.5246 ± 0.0483	0.0507	81
ROL.L	0.5253 ± 0.0462	0.5091 ± 0.0431	0.0515	302
ACG.L	0.5247 ± 0.0443	0.5078 ± 0.0394	0.0529	426
PoCG.L	0.5198 ± 0.0480	0.5029 ± 0.0404	0.0554	1159
IPL.L	0.5257 ± 0.0397	0.5104 ± 0.0406	0.0576	696
FFG.R	0.5270 ± 0.0412	0.5121 ± 0.0396	0.0592	760
LING.L	0.5180 ± 0.0496	0.5015 ± 0.0349	0.0597	660
THA.L	0.5444 ± 0.0469	0.5284 ± 0.0488	0.0664	313
PUT.R	0.5309 ± 0.0428	0.5165 ± 0.0404	0.0693	322
HIP.L	0.5383 ± 0.0497	0.5265 ± 0.0417	0.0707	273
HES.R	0.5345 ± 0.0357	0.5202 ± 0.0381	0.0771	73
PreCG.R	0.5272 ± 0.0392	0.5104 ± 0.0431	0.0898	1002
ANG.L	0.5185 ± 0.0361	0.5049 ± 0.0400	0.0917	342
PCUN.R	0.5241 ± 0.0429	0.5119 ± 0.0418	0.0919	935
LING.R	0.5155 ± 0.0392	0.5013 ± 0.0380	0.0944	678
CAL.R	0.5152 ± 0.0434	0.4992 ± 0.0378	0.0947	542
ITG.L	0.5326 ± 0.0443	0.5213 ± 0.0363	0.1030	941
ANG.R	0.5191 ± 0.0352	0.5085 ± 0.0340	0.1045	496
SFGdor.R	0.5176 ± 0.0462	0.5043 ± 0.0363	0.1114	1159
HES.L	0.5376 ± 0.0474	0.5194 ± 0.0446	0.1119	72
MFG.R	0.5138 ± 0.0456	0.5015 ± 0.0388	0.1510	1510
PUT.L	0.5295 ± 0.0401	0.5194 ± 0.0368	0.1569	306
CAL.L	0.5184 ± 0.0436	0.5073 ± 0.0355	0.1603	648
INS.R	0.5233 ± 0.0428	0.5150 ± 0.0380	0.1651	539
IFGoperc.L	0.5279 ± 0.0296	0.5176 ± 0.0399	0.1656	326
AMYG.L	0.5429 ± 0.0387	0.5355 ± 0.0487	0.1663	62
TPOsup.L	0.5469 ± 0.0319	0.5378 ± 0.0472	0.1711	382

Table 1 continued

Regions of interest	SampEn of patients	SampEn of controls	<i>p</i> value	Number of voxels
STG.R	0.5256 ± 0.0387	0.5176 ± 0.0347	0.1744	963
ORBmid.R	0.5290 ± 0.0395	0.5167 ± 0.0462	0.2037	294
ORBmid.L	0.5256 ± 0.0405	0.5164 ± 0.0364	0.2114	270
SMA.R	0.5195 ± 0.0438	0.5065 ± 0.0421	0.2271	666
PCL.R	0.5302 ± 0.0388	0.5248 ± 0.0420	0.2395	227
PCUN.L	0.5176 ± 0.0431	0.5119 ± 0.0391	0.2398	1079
ORBsupmed.L	0.5298 ± 0.0439	0.5209 ± 0.0384	0.2532	225
ITG.R	0.5330 ± 0.0358	0.5258 ± 0.0369	0.2555	1072
CUN.R	0.5217 ± 0.0410	0.5136 ± 0.0391	0.2598	434
HIP.R	0.5440 ± 0.0432	0.5383 ± 0.0469	0.2693	288
ORBinf.R	0.5276 ± 0.0413	0.5165 ± 0.0458	0.2850	505
REC.R	0.5410 ± 0.0472	0.5370 ± 0.0438	0.2893	218
PreCG.L	0.5280 ± 0.0394	0.5165 ± 0.0407	0.2964	1028
THA.R	0.5400 ± 0.0422	0.5297 ± 0.0445	0.3079	307
MFG.L	0.5180 ± 0.0413	0.5072 ± 0.0476	0.3132	1448
SMG.R	0.5134 ± 0.0288	0.5073 ± 0.0370	0.3152	550
CUN.L	0.5251 ± 0.0400	0.5176 ± 0.0365	0.3286	449
FFG.L	0.5198 ± 0.0386	0.5147 ± 0.0523	0.3550	687
PCL.L	0.5232 ± 0.0452	0.5186 ± 0.0417	0.3705	422
SFGmed.R	0.5185 ± 0.0393	0.5096 ± 0.0399	0.4227	641
ORBsup.L	0.5345 ± 0.0452	0.5269 ± 0.0502	0.4392	292
CAU.L	0.5398 ± 0.0401	0.5403 ± 0.0511	0.4441	278
TPOmid.L	0.5418 ± 0.0462	0.5350 ± 0.0422	0.4518	222
DCG.L	0.5239 ± 0.0378	0.5103 ± 0.0434	0.4608	619
SPG.L	0.5192 ± 0.0416	0.5145 ± 0.0395	0.4945	631
SMA.L	0.5188 ± 0.0456	0.5138 ± 0.0322	0.4974	656
REC.L	0.5286 ± 0.0465	0.5293 ± 0.0373	0.4985	261
MTG.L	0.5184 ± 0.0392	0.5127 ± 0.0424	0.5451	1439
OLF.L	0.5415 ± 0.0439	0.5405 ± 0.0386	0.5885	87
PCG.L	0.5264 ± 0.0418	0.5181 ± 0.0440	0.5907	137
ORBsupmed.R	0.5303 ± 0.0431	0.5241 ± 0.0387	0.6257	262
SMG.L	0.5220 ± 0.0383	0.5166 ± 0.0425	0.6266	354
MTG.R	0.5201 ± 0.0393	0.5166 ± 0.0477	0.6302	1356
PHG.L	0.5433 ± 0.0440	0.5392 ± 0.0457	0.6477	286
ORBsup.R	0.5287 ± 0.0417	0.5272 ± 0.0455	0.7148	311
PHG.R	0.5456 ± 0.0373	0.5368 ± 0.0456	0.7353	316
ORBinf.L	0.5219 ± 0.0398	0.5217 ± 0.0399	0.8062	503
TPOsup.R	0.5349 ± 0.0419	0.5317 ± 0.0389	0.8151	400
CAU.R	0.5435 ± 0.0469	0.5449 ± 0.0518	0.8171	284
IFGoperc.R	0.5230 ± 0.0428	0.5201 ± 0.0391	0.8177	421
IFGtriang.R	0.5259 ± 0.0418	0.5262 ± 0.0421	0.8262	629
SFGmed.L	0.5164 ± 0.0406	0.5156 ± 0.0383	0.8574	846
AMYG.R	0.5365 ± 0.0373	0.5402 ± 0.0438	0.8586	70
DCG.R	0.5194 ± 0.0421	0.5091 ± 0.0443	0.8627	605

Table 1 continued

	Regions of interest	SampEn of patients	SampEn of controls	<i>p</i> value	Number of voxels
Significant <i>p</i> values are indicated by asterisks	TPOmid.R	0.5369 ± 0.0495	0.5369 ± 0.0455	0.8779	349
	IPL.R	0.5139 ± 0.0437	0.5118 ± 0.0402	0.9249	419

Firstly, we construct embedding vectors $\mathbf{v}_i = (x_i, x_{i+1}, \dots, x_{i+m-1})$ ($1 \leq i \leq N - m + 1$), where m represents the dimension of \mathbf{v}_i .

Secondly, for each i , we define

$$C_i^m = \frac{1}{N - m} \sum_{j=1, j \neq i}^{N-m+1} \Theta(r - \|v_i - v_j\|). \tag{1}$$

Here, r represents a tolerance value which is defined as $r = \varepsilon \cdot \sigma_x$, where ε stands for a small parameter and σ_x represents the standard deviation of \mathbf{x} . $\Theta(\cdot)$ is defined as

$$\Theta(x) = \begin{cases} 0, & x < 0; \\ 1, & x \geq 0. \end{cases} \tag{2}$$

$\|\cdot\|$ stands for the Chebyshev distance, i.e.,

$$\|v_i - v_j\| = \max(|x_i - x_j|, |x_{i+1} - x_{j+1}|, \dots, |x_{i+m-1} - x_{j+m-1}|). \tag{3}$$

Similarly, we define

$$C_i^{m+1} = \frac{1}{N - m - 1} \sum_{j=1, j \neq i}^{N-m} \Theta(r - \|v_i - v_j\|). \tag{4}$$

Thirdly, by averaging across different values of i , we obtain

$$U^m = \frac{1}{N - m + 1} \sum_{i=1}^{N-m+1} C_i^m, \tag{5}$$

and

$$U^{m+1} = \frac{1}{N - m} \sum_{i=1}^{N-m} C_i^{m+1}. \tag{6}$$

Finally, we calculate SampEn of \mathbf{x} as

$$\text{SampEn} = -\ln \frac{U^{m+1}}{U^m}. \tag{7}$$

The values of SampEn are nonnegative, and larger values of SampEn mean more irregularity or complexity [51]. Previous studies showed that the values of SampEn exhibited good statistical properties when $m = 1$ or 2 [52] and ε was in the range from 0.1 to

0.25 [15]. Previous studies also showed that $m = 2$ allowed more detailed reconstruction of the joint probabilistic dynamics [53]. Hence, m is fixed at 2 throughout this study. Our previous study showed that changes of SampEn of dynamic functional connectivity time series were not sensitive to values of ε in the range from 0.1 to 0.25 [45]. Thus, ε is fixed at 0.2 throughout this study.

2.5 SampEn at different levels of the brain

For each participant, after calculating SampEn of 4005 dynamic functional connections, SampEn of 90 regions of interest, of 6 resting-state networks, and of the whole brain is further calculated, respectively. SampEn of a region of interest is defined as the mean of SampEn of 89 dynamic functional connections related to it. According to the previous study [54], the whole brain was divided into 6 resting-state networks, including the default mode network, the attention network, the visual recognition network, the auditory network, the sensory-motor network, and the subcortical network. The default mode network, the attention network, the visual recognition network, the auditory network, the sensory-motor network, and the subcortical network are composed of 20, 16, 14, 12, 8, and 20 regions of interest, respectively. Regions of interest in each resting-state network can be found in Table S2 of Ref. [45]. SampEn of a resting-state network is defined as the mean of SampEn of all regions of interest in the resting-state network. SampEn of the whole brain is defined as the mean of SampEn of all regions of interest in the brain.

2.6 Statistical analysis

The difference in demographic characteristics between the patients and the controls is assessed by two-tailed, two-sample t tests or χ^2 tests where appropriate. Specifically, the difference in age and in education is assessed by t tests, whereas the difference in

Table 2 Demographic characteristics

	Patients	Controls	<i>p</i> value
Gender (male/female)	35/34	25/27	0.23
Age (years)	31.95 ± 9.60	29.87 ± 8.62	0.28
Education (years)	14.19 ± 2.16	15.29 ± 2.39	0.01*
Illness duration (years)	7.17 ± 6.61	—	—
Positive scale	11.92 ± 4.71	—	—
Negative scale	13.61 ± 6.33	—	—
General scale	27.28 ± 9.64	—	—

P values which are less than 0.05 are indicated by asterisks

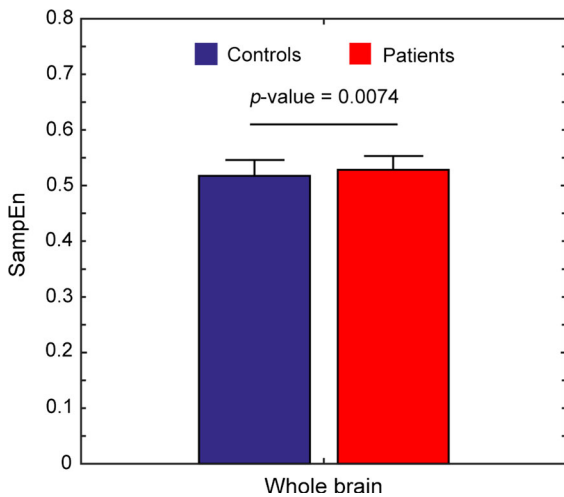


Fig. 2 The mean SampEn of the whole brain over all controls and over all patients. The error bars represent standard deviations

gender is assessed by χ^2 tests. The significance levels of the tests are characterized by *p* values, with larger *p* values corresponding to higher significance levels.

To study the difference in SampEn between the patients and the controls, two-tailed, two-sample *t* tests on SampEn at different levels of the brain are performed, with gender, age, education, and head motion as covariates. The significance levels of the *t* tests are also characterized by *p* values. First, *t* tests on SampEn of the whole brain and of the resting-state networks are performed. Then, for each resting-state network, *t* tests on SampEn of all regions of interest in the resting-state network are performed. Because there are 6 resting-state networks and each resting-state network is composed of many regions of interest, corrections for multiple comparisons are needed for *t* tests on SampEn of resting-state networks and of regions of interest. False discovery rate (FDR) corrections are applied to correct for multiple comparisons [55].

To explore whether the changed SampEn in the patients is associated with the characteristics of schizophrenia, the relationship between SampEn and clinical variables such as PANSS and illness duration is studied. Partial correlation analyses are applied to study these relationships, controlling for the influence of gender, age, education, and head motion. The significance levels of the partial correlation analyses are also characterized by *p* values. The patients who do not finish their PANSS evaluation are excluded from the partial correlation analyses.

Table 3 SampEn at different levels of the brain in the patients is significantly higher than that in the controls

	SampEn of patients	SampEn of controls	<i>p</i> value
Whole brain	0.5282 ± 0.0285	0.5174 ± 0.0248	0.0074
Resting-state networks			
VRN	0.5238 ± 0.0260	0.5078 ± 0.0237	0.0015
AUN	0.5298 ± 0.0239	0.5171 ± 0.0258	0.0108
Regions of interest			
MOG. L	0.5263 ± 0.0380	0.5037 ± 0.0433	0.0014
MOG. R	0.5351 ± 0.0387	0.5094 ± 0.0399	0.0024
IOG. R	0.5352 ± 0.0420	0.5110 ± 0.0379	0.0033
SOG. L	0.5242 ± 0.0424	0.5060 ± 0.0349	0.0057
ROL. R	0.5354 ± 0.0458	0.5048 ± 0.0359	0.0009

VRN visual recognition network, AUN auditory network, MOG. L left middle occipital gyrus, MOG. R right middle occipital gyrus, IOG. R right inferior occipital gyrus, SOG. L left superior occipital gyrus, ROL. R right rolandic operculum

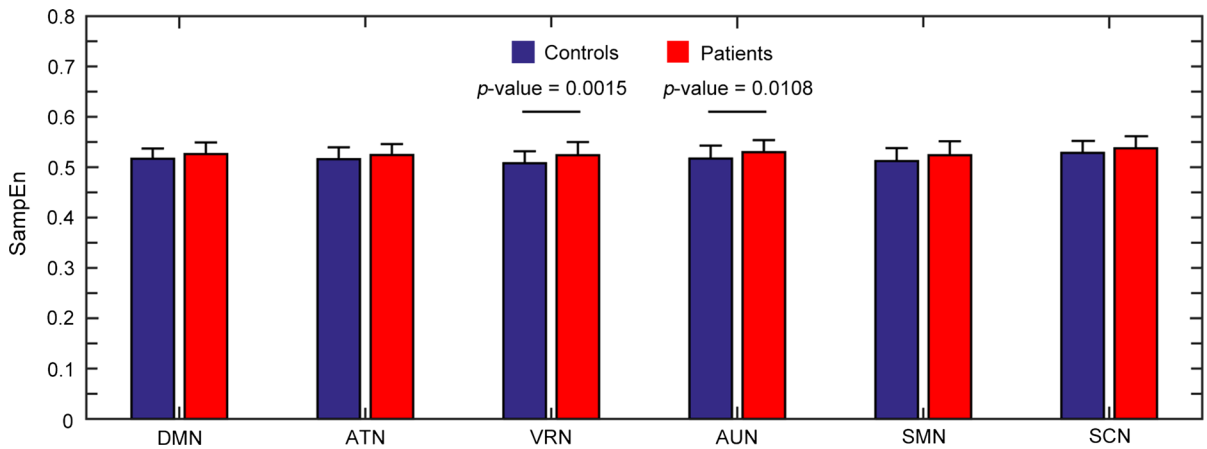


Fig. 3 The mean SampEn of each of 6 resting-state networks over all controls and over all patients. The error bars stand for standard deviations. After FDR controls, resting-state networks with p values below 0.025 are deemed to be significant. *DMN*

default mode network, *ATN* attention network, *VRN* visual recognition network, *AUN* auditory network, *SMN* sensory-motor network, *SCN* subcortical network

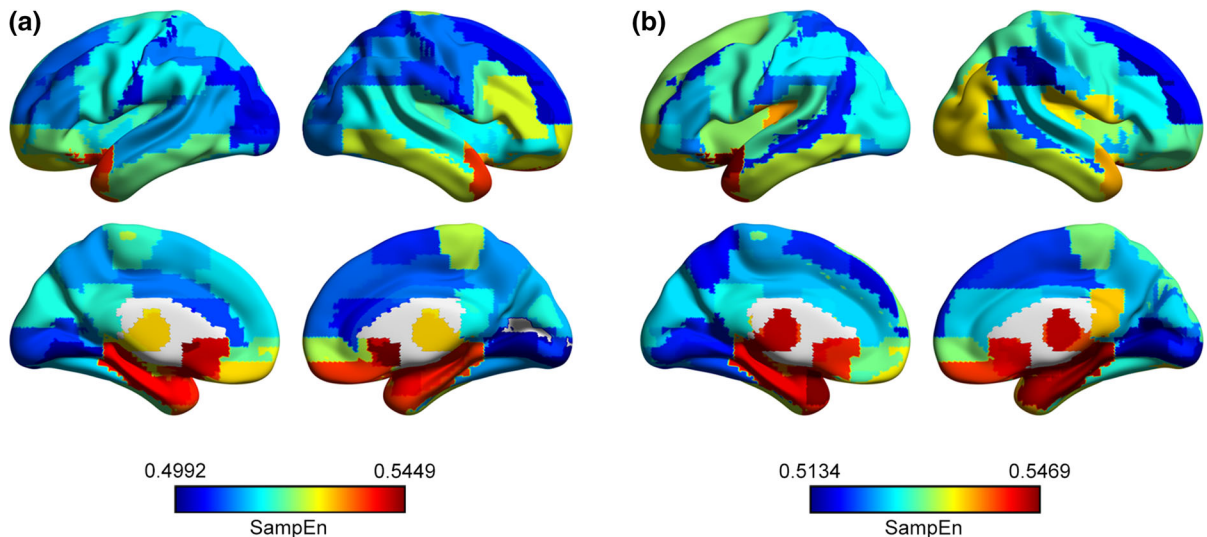


Fig. 4 The mean SampEn of each region of interest over all controls (a) and over all patients (b). The color bars indicate the values of SampEn. (Color figure online)

3 Results

3.1 Demographic characteristics of the participants

Details of the participants' demographic characteristics are displayed in Table 2. Except that the patients have a shorter education duration (p value < 0.05), which is caused by schizophrenia, the patients and the controls are matched by gender (p value > 0.05) and age (p value > 0.05). The illness duration, the positive scale, the negative scale, and the general scale

are important clinical variables for characterizing the symptoms of patients. Correlation analyses on SampEn and these clinical variables are studied in Sect. 3.5 to identify the relationship between SampEn and characteristics of schizophrenia. In Table 2, the values before and after the symbols \pm represent the means and the standard deviations, respectively. The means and the standard deviations of the positive scale, the negative scale, and the general scale are obtained from the data of the patients who finish their PANSS evaluation.

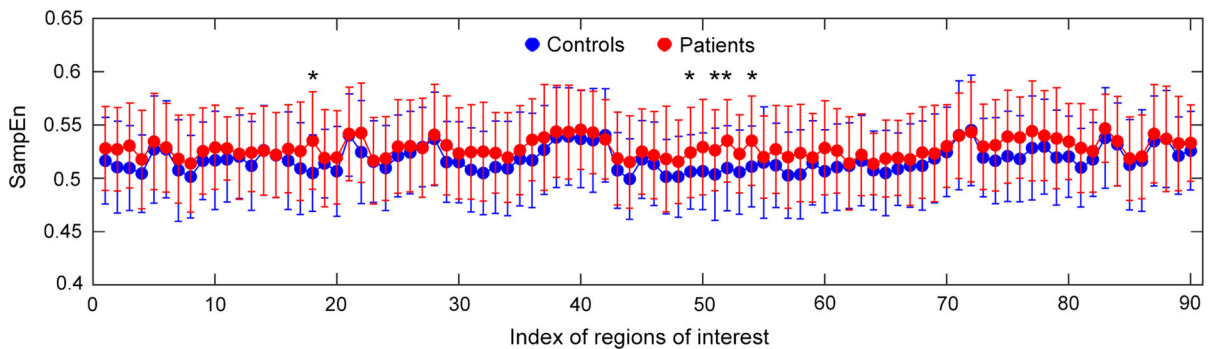


Fig. 5 The mean SampEn of each region of interest over all controls and over all patients. The error bars represent standard deviations. Regions of interest showing significant effects are

indicated by asterisks. The full name of each region of interest can be found in Table S1 of Ref. [45]

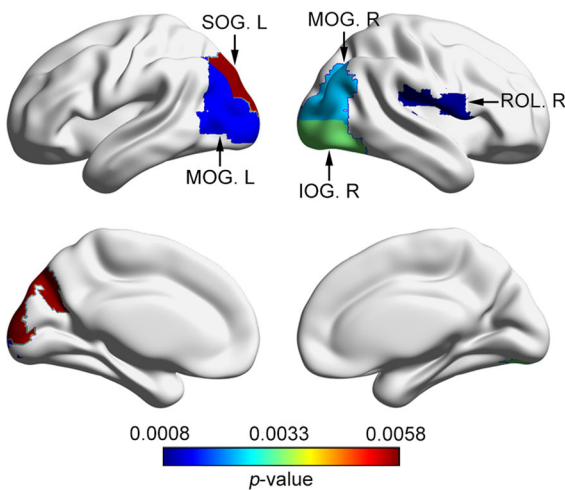


Fig. 6 SampEn of the left middle occipital gyrus (MOG. L), the right middle occipital gyrus (MOG. R), the right inferior occipital gyrus (IOG. R), the left superior occipital gyrus (SOG. L), and the right Rolandic operculum (ROL. R) in the patients is significantly higher than that in the controls. The color bar represents the p value. After FDR controls, regions of interest in the visual recognition network with p values below 0.0179 are considered to be significant, whereas regions of interest in the auditory network with p values below 0.0083 are deemed to be significant. (Color figure online)

3.2 Higher SampEn at the whole-brain level of the patients' brain

The mean SampEn of the whole brain over all controls and over all patients is 0.5174 and 0.5282, respectively (Fig. 2 and Table 3). The patients show significantly higher SampEn than the controls (p value < 0.05 ; Fig. 2 and Table 3). In Table 3, values before and after the symbols \pm represent mean values and standard deviations, respectively.

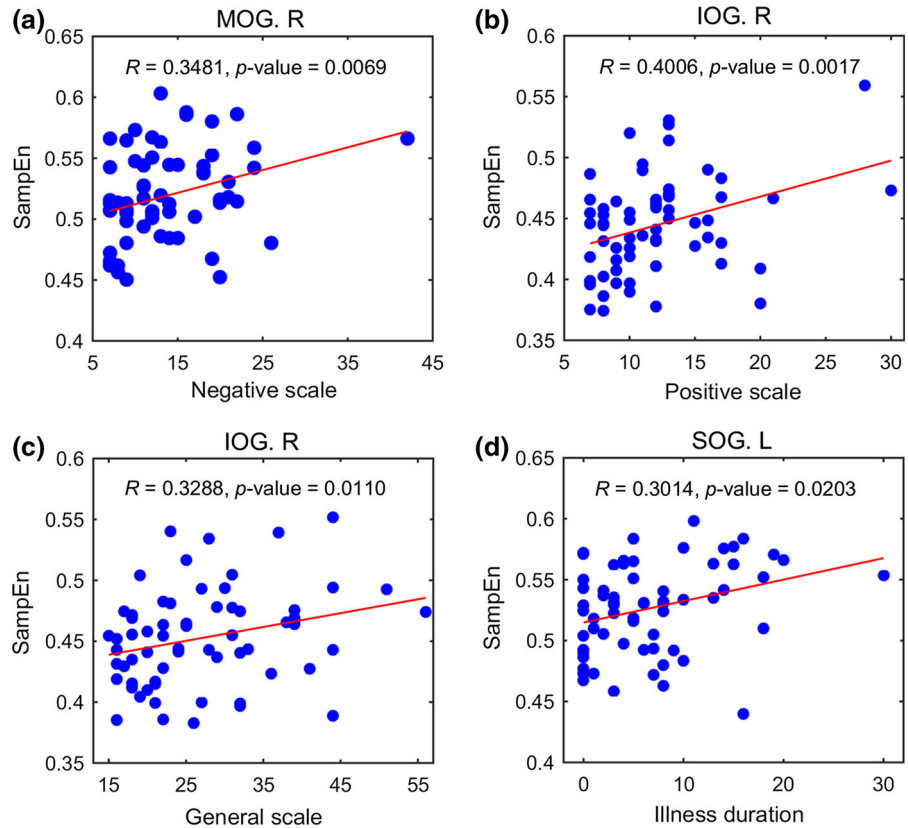
3.3 Higher SampEn at the network level of the patients' brain

The mean SampEn of a resting-state network over all controls and over all patients is in the range from 0.5078 to 0.5283 and in the range from 0.5238 to 0.5374, respectively (Fig. 3). The mean SampEn of the visual recognition network over all controls and over all patients is, respectively, 0.5078 and 0.5238, and the mean SampEn of the auditory network over all controls and over all patients is, respectively, 0.5171 and 0.5298 (Table 3 and Fig. 3). For the visual recognition network and the auditory network, the patients exhibit significantly higher SampEn than the controls (p value < 0.05 , FDR corrected; Table 3 and Fig. 3). However, for the other 4 resting-state networks (the default mode network, the attention network, the sensory-motor network, and the subcortical network), there is no significant difference in SampEn between the two groups (p value > 0.05 , FDR corrected). This suggests that for the patients, the significantly higher SampEn of the whole brain is caused by the significantly higher SampEn of the visual recognition network and the auditory network.

3.4 Higher SampEn at the regional level of the patients' brain

The mean SampEn of a region of interest over all controls and over all patients, respectively, ranges from 0.4992 to 0.5449 and from 0.5134 to 0.5469 (Fig. 4). The detailed SampEn value of each region of interest is shown in Table 1 and Fig. 5. For some regions

Fig. 7 Significant positive correlations between SampEn of regions of interest and clinical variables. **a** SampEn of the right middle occipital gyrus (MOG. R) and the negative scale. **b** SampEn of the right inferior occipital gyrus (IOG. R) and the positive scale. **c** SampEn of the right inferior occipital gyrus (IOG. R) and the general scale. **d** SampEn of the left superior occipital gyrus (SOG. L) and the illness duration. R represents the correlation coefficient



of interest in the visual recognition network and in the auditory network, the patients display significantly higher SampEn than the controls. In the visual recognition network, regions of interest showing significant effects are the left middle occipital gyrus, the right middle occipital gyrus, the right inferior occipital gyrus, and the left superior occipital gyrus (p value < 0.05, FDR corrected; Table 3, Fig. 5, and Fig. 6). In the auditory network, only the right rolandic operculum shows significant effects (p value < 0.05, FDR corrected; Table 3, Fig. 5, and Fig. 6). For regions of interest in other 4 resting-state networks, no significant differences in SampEn between the two groups are identified (p value > 0.05, FDR corrected). This implies that these 5 regions of interest mainly determine the difference in SampEn between the patients and the controls.

3.5 Positive correlation between SampEn and clinical variables

For the whole brain, the 2 significant resting-state networks, and the 5 significant regions of interest, we per-

form partial correlation analyses between SampEn and clinical variables to identify the relationship between SampEn and characteristics of the schizophrenia, controlling for the effect of gender, age, education, and head motion. Although SampEn of the whole brain, of the visual recognition network, and of the auditory network is not correlated with the clinical variables, SampEn of 3 out of 5 regions of interest shows a strong positive correlation with the clinical variables. The 3 regions of interest are the right middle occipital gyrus, the right inferior occipital gyrus, and the left superior occipital gyrus. Specifically, SampEn of the right middle occipital gyrus is significantly and positively correlated with the negative scale (p value < 0.05; Fig. 7a). SampEn of the right inferior occipital gyrus shows significant positive correlations with the positive scale and with the general scale (p value < 0.05; Fig. 7b, 7c). SampEn of the left superior occipital gyrus is significantly and positively correlated with the illness duration (p value < 0.05; Fig. 7d). Detailed results of the partial correlation analyses are shown in Table 4.

Table 4 Partial correlation analyses between SampEn and clinical variables

	Positive scale		Negative scale		General scale		Illness duration	
	<i>R</i>	<i>p</i> value	<i>R</i>	<i>p</i> value	<i>R</i>	<i>p</i> value	<i>R</i>	<i>p</i> value
Whole brain	0.1117	0.3996	0.1314	0.3211	−0.0327	0.8059	−0.0212	0.8736
VRN	0.1970	0.1347	0.2313	0.0780	0.0567	0.6697	0.1182	0.3728
AUN	0.1136	0.3916	0.0982	0.4592	−0.0424	0.7498	0.0778	0.5582
MOG. L	−0.0006	0.9962	0.1504	0.2556	0.0608	0.6476	0.0224	0.8661
MOG. R	−0.0539	0.6851	0.3481	0.0069*	0.0778	0.5581	0.1091	0.4107
IOG. R	0.4006	0.0017*	0.2434	0.0632	0.3288	0.0110*	0.0297	0.8231
SOG. L	0.0546	0.6815	0.0183	0.8904	0.0070	0.9582	0.3014	0.0203*
ROL. R	−0.0128	0.9234	−0.0300	0.8218	−0.1127	0.3954	0.0543	0.6831

R represents the correlation coefficient. *VRN* visual recognition network, *AUN* auditory network, *MOG. L* left middle occipital gyrus, *MOG. R* right middle occipital gyrus, *IOG. R* right inferior occipital gyrus, *SOG. L* left superior occipital gyrus, *ROL. R* right rolandic operculum

P values which are less than 0.05 are indicated by asterisks

4 Conclusion and discussion

In the present paper, the nonlinear properties of functional brain networks of patients with schizophrenia are characterized by SampEn of dynamic functional connectivity. It is shown that the visual cortex of the patients with schizophrenia exhibits significantly higher SampEn than that of the healthy controls. This is consistent with previous studies on nonlinear properties of brain signals measured by different techniques. For example, Fernandez et al. used Lempel-Ziv complexity to characterize the nonlinear properties of resting-state MEG signals of patients with schizophrenia and of healthy controls, and found that patients showed significantly higher complexity as compared to controls [11]. Sokunbi et al. used SampEn to identify the nonlinear properties of BOLD signals of patients with schizophrenia and of healthy controls while performing the cyberball social exclusion task, and showed that patients exhibited significantly higher complexity than controls [14]. Because nonlinear properties are important indices in describing the nonlinearity, these previous studies along with our study further validate the notion that the nonlinearity underlies the irregularity in psychotic symptoms of schizophrenia [56]. Moreover, we also show that the changed SampEn of patients with schizophrenia is associated with the illness duration or the symptom severity scores. These results indicate that nonlinear properties are effective biomarkers in characterizing

the brain functional networks of patients with brain disorders.

In our previous study [45], the association between SampEn of dynamic functional connectivity and age was investigated. It was demonstrated that SampEn of the amygdala–cortical connectivity decreased with advancing age, and this age-related loss disappeared in patients with schizophrenia. Different from our previous study, the present study examines the effect of schizophrenia on SampEn of dynamic functional connectivity by analyzing the difference in SampEn between patients with schizophrenia and healthy controls. It is demonstrated that the patients show significantly higher SampEn than the controls at different levels of the brain, which is mainly caused by a significantly higher SampEn in the visual cortex of the patients. In addition, it is also demonstrated that SampEn of the visual cortex of the patients is significantly and positively associated with the illness duration or the symptom severity scores.

As suggested by our finding that the visual cortex of the patients with schizophrenia exhibits significantly higher SampEn than that of the healthy controls, the visual cortex should be related to schizophrenia. This is in line with many earlier researches on static functional connectivity, which showed that functional connectivity corresponding to the visual cortex changed in patients with schizophrenia [57–60]. Our study and these previous studies help to understand abnormal visual functions in patients with schizophrenia such as visual hallucinations. In addition to the visual cortex,

by using different samples of patients with schizophrenia, previous studies showed that some other brain regions were also related to schizophrenia [33–36]. In the future, nonlinear analysis should be extensively used to study the components as well as the dynamic properties of brain functional networks.

Compliance with ethical standard

Conflict of interest The authors declare that they have no conflict of interest.

References

- Elbert, T., Ray, W.J., Kowalik, Z.J., Skinner, J.E., Graf, K.E., Birbaumer, N.: Chaos and physiology: deterministic chaos in excitable cell assemblies. *Physiol. Rev.* **74**, 1–47 (1994)
- Gu, H.G., Pan, B.B., Chen, G.R., Duan, L.X.: Biological experimental demonstration of bifurcations from bursting to spiking predicted by theoretical models. *Nonlinear Dyn.* **78**, 391–407 (2014)
- Li, Y.Y., Gu, H.G.: The distinct stochastic and deterministic dynamics between period-adding and period-doubling bifurcations of neural bursting patterns. *Nonlinear Dyn.* **87**, 2541–2562 (2017)
- Shilnikov, A.: Complete dynamical analysis of a neuron model. *Nonlinear Dyn.* **68**, 305–328 (2012)
- van Vreeswijk, C., Sompolinsky, H.: Chaos in neuronal networks with balanced excitatory and inhibitory activity. *Science* **274**, 1724–1726 (1996)
- Buzsaki, G., Draguhn, A.: Neuronal oscillations in cortical networks. *Science* **304**, 1926–1929 (2004)
- Ma, J., Hu, B.L., Wang, C.N., Jin, W.Y.: Simulating the formation of spiral wave in the neuronal system. *Nonlinear Dyn.* **73**, 73–83 (2013)
- Ma, J., Tang, J.: A review for dynamics in neuron and neuronal network. *Nonlinear Dyn.* **89**, 1569–1578 (2017)
- Wang, G.P., Jin, W.Y., Wang, A.: Synchronous firing patterns and transitions in small-world neuronal network. *Nonlinear Dyn.* **81**, 1453–1458 (2015)
- Wang, X.J.: Neurophysiological and computational principles of cortical rhythms in cognition. *Physiol. Rev.* **90**, 1195–1268 (2010)
- Fernandez, A., Lopez-Ibor, M.I., Turrero, A., Santos, J.M., Moron, M.D., Hornero, R., Gomez, C., Mendez, M.A., Ortiz, T., Lopez-Ibor, J.J.: Lempel-Ziv complexity in schizophrenia: a MEG study. *Clin. Neurophysiol.* **122**, 2227–2235 (2011)
- Liu, C.Y., Krishnan, A.P., Yan, L.R., Smith, R.X., Kilroy, E., Alger, J.R., Ringman, J.M., Wang, D.J.J.: Complexity and synchronicity of resting state blood oxygenation level-dependent (BOLD) functional MRI in normal aging and cognitive decline. *J. Magn. Reson. Imaging* **38**, 36–45 (2013)
- Maksimenko, V.A., Pavlov, A., Runnova, A.E., Nedaivozov, V., Grubov, V., Koronovslii, A., Pchelintseva, S.V., Pitsik, E., Pisarchik, A.N., Hramov, A.E.: Nonlinear analysis of brain activity, associated with motor action and motor imaginary in untrained subjects. *Nonlinear Dyn.* **91**, 2803–2817 (2018)
- Wang, Z., Li, Y., Childress, A.R., Detre, J.A.: Brain entropy mapping using fMRI. *Plos One* **9**, e89948 (2014)
- Sokunbi, M.O.: Sample entropy reveals high discriminative power between young and elderly adults in short fMRI data sets. *Front. Neuroinform.* **8**, 69 (2014)
- Sokunbi, M.O., Gradin, V.B., Waiter, G.D., Cameron, G.G., Ahearn, T.S., Murray, A.D., Steele, D.J., Staff, R.T.: Nonlinear complexity analysis of brain fMRI signals in schizophrenia. *Plos One* **9**, e95146 (2014)
- Yan, J.Q., Wang, Y.H., Ouyang, G.X., Yu, T., Li, Y.J., Sik, A., Li, X.L.: Analysis of electrocorticogram in epilepsy patients in terms of criticality. *Nonlinear Dyn.* **83**, 1909–1917 (2016)
- Yang, A.C., Huang, C.C., Yeh, H.L., Liu, M.E., Hong, C.J., Tu, P.C., Chen, J.F., Huang, N.E., Peng, C.K., Lin, C.P., Tsai, S.J.: Complexity of spontaneous BOLD activity in default mode network is correlated with cognitive function in normal male elderly: a multiscale entropy analysis. *Neurobiol. Aging* **34**, 428–438 (2013)
- Yeh, C.H., Shi, W.B.: Generalized multiscale Lempel-Ziv complexity of cyclic alternating pattern during sleep. *Nonlinear Dyn.* **93**, 1899–1910 (2018)
- Deco, G., Jirsa, V.K.: Ongoing cortical activity at rest: criticality, multistability, and ghost attractors. *J. Neurosci.* **32**, 3366–3375 (2012)
- Biswal, B., Yetkin, F.Z., Haughton, V.M., Hyde, J.S.: Functional connectivity in the motor cortex of resting human brain using echo-planar MRI. *Magn. Reson. Med.* **34**, 537–541 (1995)
- Eguiluz, V.M., Chialvo, D.R., Cecchi, G.A., Baliki, M., Apkarian, A.V.: Scale-free brain functional networks. *Phys. Rev. Lett.* **94**, 018102 (2005)
- Fox, M.D., Raichle, M.E.: Spontaneous fluctuations in brain activity observed with functional magnetic resonance imaging. *Nat. Rev. Neurosci.* **8**, 700–711 (2007)
- Sheffield, J.M., Barch, D.M.: Cognition and resting-state functional connectivity in schizophrenia. *Neurosci. Biobehav. R.* **61**, 108–120 (2016)
- Hull, J.V., Dokovna, L.B., Jacokes, Z.J., Torgerson, C.M., Irimia, A., Van Horn, J.D.: Resting-state functional connectivity in autism spectrum disorders: a review. *Front. Psychiatry* **7**, 205 (2016)
- Mulders, P.C., van Eijndhoven, P.F., Schene, A.H., Beckmann, C.F., Tendolkar, I.: Resting-state functional connectivity in major depressive disorder: a review. *Neurosci. Biobehav. R.* **56**, 330–344 (2015)
- Wang, R., Wang, L., Yang, Y., Li, J.J., Wu, Y., Lin, P.: Random matrix theory for analyzing the brain functional network in attention deficit hyperactivity disorder. *Phys. Rev. E* **94**, 052411 (2016)
- Friston, K.J., Frith, C.D., Liddle, P.F., Frackowiak, R.S.: Functional connectivity: the principal-component analysis of large (PET) data sets. *J. Cerebr. Blood F. Met.* **13**, 5–14 (1993)
- Bullmore, E., Sporns, O.: The economy of brain network organization. *Nat. Rev. Neurosci.* **13**, 336–349 (2012)
- Cheng, W., Rolls, E.T., Gu, H.G., Zhang, J., Feng, J.F.: Autism: reduced connectivity between cortical areas involved in face expression, theory of mind, and the sense of self. *Brain* **138**, 1382–1393 (2015)

31. Takahashi, T.: Complexity of spontaneous brain activity in mental disorders. *Prog. Neuro-Psychoph.* **45**, 258–266 (2013)
32. Cabral, J., Fernandes, H.M., Van Hartevelt, T.J., James, A.C., Kringelbach, M.L., Deco, G.: Structural connectivity in schizophrenia and its impact on the dynamics of spontaneous functional networks. *Chaos* **23**, 046111 (2013)
33. Cheng, W., Palaniyappan, L., Li, M., Kendrick, K.M., Zhang, J., Luo, Q., Liu, Z., Yu, R., Deng, W., Wang, Q., Ma, X., Guo, W., Francis, S., Liddle, P., Mayer, A.R., Schumann, G., Li, T., Feng, J.: Voxel-based, brain-wide association study of aberrant functional connectivity in schizophrenia implicates thalamocortical circuitry. *NPJ. Schizophrenia* **1**, 15016 (2015)
34. Lynall, M.E., Bassett, D.S., Kerwin, R., McKenna, P.J., Kitzbichler, M., Muller, U., Bullmore, E.: Functional connectivity and brain networks in schizophrenia. *J. Neurosci.* **30**, 9477–9487 (2010)
35. Manoliu, A., Riedl, V., Zherdin, A., Muhlau, M., Schwerthoffer, D., Scherr, M., Peters, H., Zimmer, C., Forstl, H., Bauml, J., Wohlschlagler, A.M., Sorg, C.: Aberrant dependence of default mode/central executive network interactions on anterior insular salience network activity in schizophrenia. *Schizophrenia Bull.* **40**, 428–437 (2014)
36. Whitfield-Gabrieli, S., Thermenos, H.W., Milanovic, S., Tsuang, M.T., Faraone, S.V., McCarley, R.W., Shenton, M.E., Green, A.I., Nieto-Castanon, A., LaViolette, P., Wojcik, J., Gabrieli, J.D., Seidman, L.J.: Hyperactivity and hyperconnectivity of the default network in schizophrenia and in first-degree relatives of persons with schizophrenia. *P. Natl. Acad. Sci. USA* **106**, 1279–1284 (2009)
37. Allen, E.A., Damaraju, E., Plis, S.M., Erhardt, E.B., Eichele, T., Calhoun, V.D.: Tracking whole-brain connectivity dynamics in the resting state. *Cereb. Cortex* **24**, 663–676 (2014)
38. Chang, C., Glover, G.H.: Time-frequency dynamics of resting-state brain connectivity measured with fMRI. *NeuroImage* **50**, 81–98 (2010)
39. Hutchison, R.M., Womelsdorf, T., Gati, J.S., Everling, S., Menon, R.S.: Resting-state networks show dynamic functional connectivity in awake humans and anesthetized macaques. *Hum. Brain Mapp.* **34**, 2154–2177 (2013)
40. Kaiser, R.H., Whitfield-Gabrieli, S., Dillon, D.G., Goer, F., Beltzer, M., Minkel, J., Smoski, M., Dichter, G., Pizzagalli, D.A.: Dynamic resting-state functional connectivity in major depression. *Neuropsychopharmacol.* **41**, 1822–1830 (2016)
41. Marusak, H.A., Calhoun, V.D., Brown, S., Crespo, L.M., Sala-Hamrick, K., Gotlib, I.H., Thomason, M.E.: Dynamic functional connectivity of neurocognitive networks in children. *Hum. Brain Mapp.* **38**, 97–108 (2017)
42. Rashid, B., Damaraju, E., Pearlson, G.D., Calhoun, V.D.: Dynamic connectivity states estimated from resting fMRI identify differences among schizophrenia, bipolar disorder, and healthy control subjects. *Front. Hum. Neurosci.* **8**, 897 (2014)
43. Wang, R., Zhang, Z.Z., Ma, J., Yang, Y., Lin, P., Wu, Y.: Spectral properties of the temporal evolution of brain network structure. *Chaos* **25**, 123112 (2015)
44. Zhang, J., Cheng, W., Liu, Z., Zhang, K., Lei, X., Yao, Y., Becker, B., Liu, Y., Kendrick, K.M., Lu, G., Feng, J.: Neural, electrophysiological and anatomical basis of brain-network variability and its characteristic changes in mental disorders. *Brain* **139**, 2307–2321 (2016)
45. Jia, Y., Gu, H., Luo, Q.: Sample entropy reveals an age-related reduction in the complexity of dynamic brain. *Sci. Rep.* **7**, 7990 (2017)
46. <http://www.fil.ion.ucl.ac.uk/spm>. Accessed 20 Apr 2018
47. Yan, C.G., Zang, Y.F.: DPARSF: a MATLAB toolbox for pipeline data analysis of resting-state fMRI. *Front. Syst. Neurosci.* **4**, 13 (2010)
48. Tzourio-Mazoyer, N., Landeau, B., Papathanassiou, D., Crivello, F., Etard, O., Delcroix, N., Mazoyer, B., Joliot, M.: Automated anatomical labeling of activations in SPM using a macroscopic anatomical parcellation of the MNI MRI single-subject brain. *NeuroImage* **15**, 273–289 (2002)
49. Shirer, W.R., Ryali, S., Rykhlevskaia, E., Menon, V., Greicius, M.D.: Decoding subject-driven cognitive states with whole-brain connectivity patterns. *Cereb. Cortex* **22**, 158–165 (2012)
50. Li, X., Zhu, D., Jiang, X., Jin, C., Zhang, X., Guo, L., Zhang, J., Hu, X., Li, L., Liu, T.: Dynamic functional connectomics signatures for characterization and differentiation of PTSD patients. *Hum. Brain Mapp.* **35**, 1761–1778 (2014)
51. Richman, J.S., Moorman, J.R.: Physiological time-series analysis using approximate entropy and sample entropy. *Am. J. Physiol. Heart. C.* **278**, H2039–H2049 (2000)
52. Pincus, S.M.: Assessing serial irregularity and its implications for health. *Ann. NY. Acad. Sci.* **954**, 245–267 (2001)
53. Pincus, S.M., Goldberger, A.L.: Physiological time—series analysis—what does regularity quantify. *Am. J. Physiol.* **266**, H1643–H1656 (1994)
54. Guo, S., Kendrick, K.M., Yu, R., Wang, H.L., Feng, J.: Key functional circuitry altered in schizophrenia involves parietal regions associated with sense of self. *Hum. Brain Mapp.* **35**, 123–139 (2014)
55. Benjamini, Y., Hochberg, Y.: Controlling the false discovery rate—a practical and powerful approach to multiple testing. *J. Roy. Stat. Soc. B.* **57**, 289–300 (1995)
56. Breakspear, M.: The nonlinear theory of schizophrenia. *Aust. NZ. J. Psychiat.* **40**, 20–35 (2006)
57. Hoptman, M.J., Zuo, X.N., D’Angelo, D., Mauro, C.J., Butler, P.D., Milham, M.P., Javitt, D.C.: Decreased interhemispheric coordination in schizophrenia: a resting state fMRI study. *Schizophr. Res.* **141**, 1–7 (2012)
58. Kyriakopoulos, M., Dima, D., Roiser, J.P., Corrigall, R., Barker, G.J., Frangou, S.: Abnormal functional activation and connectivity in the working memory network in early-onset schizophrenia. *J. Am. Acad. Child Psy.* **51**, 911–920 (2012)
59. White, T., Schmidt, M., Kim, D.I., Calhoun, V.D.: Disrupted functional brain connectivity during verbal working memory in children and adolescents with schizophrenia. *Cereb. Cortex* **21**, 510–518 (2011)
60. Zhuo, C., Zhu, J., Qin, W., Qu, H., Ma, X., Tian, H., Xu, Q., Yu, C.: Functional connectivity density alterations in schizophrenia. *Front. Behav. Neurosci.* **8**, 404 (2014)

Publisher’s Note Springer Nature remains neutral with regard to jurisdictional claims in published maps and institutional affiliations.